Damage Detection in Asymmetric Buildings using Vibration based Techniques

Y. Wang[1], D.P. Thambiratnam[1], T.H.T. Chan[1], A. Nguyen[2]

[1]*School of Civil Engineering and Built Environment, Queensland University of Technology, Brisbane, Australia*

[2]*School of Civil Engineering and Surveying, University of Southern Queensland, Springfield, Australia*

ABSTRACT

In recent times, aesthetic and functionality requirements have caused many buildings to be asymmetric. An asymmetric building can be defined as one in which there is either geometric, stiffness or mass eccentricity. Such buildings exhibit complex vibrations as there is coupling between the lateral and torsional components of vibration, and are referred to as torsionally coupled buildings. These building require three dimensional modelling and analysis. Despite recent research and successful applications of damage detection techniques in civil structures, assessing damage in asymmetric buildings remains a challenging task for structural engineers. There has been considerably less investigation on the methodologies for detecting and locating damage specific to torsionally coupled asymmetric buildings. This paper develops a Multi-Criteria Approach (MCA) using vibration based damage indices for detecting and locating damage in asymmetric building structures. These vibration indices are based on the modified versions of the Modal Flexibility (MF) and the Modal Strain Energy (MSE) methods. The proposed procedure is first validated through experimental testing of a laboratory scale asymmetric building model. Numerically simulated modal data of a larger scale asymmetric building obtained from finite element analysis of the intact and damaged asymmetric building models are then applied into the modified MF and modal MSE algorithms for detecting and locating the damage. Results show that the proposed method is capable of detecting both single and multiple damages in the beams and columns of asymmetric building structures.

KEYWORDS: Asymmetric building, modal flexibility, modal strain energy, structural damage, vibration based damage detection, finite element method

1. INTRODUCTION

Building structures deteriorate with time and continuously accumulate damage during their service lives due to environmental effects, changes in load distributions and natural hazards such as impacts, earthquakes, storms and corrosion. If such damage is undetected, it might cause structural failure and lead to loss of human lives. It is therefore important to detect the structural damage before failure occurs. Structural Health Monitoring (SHM) is a viable technology to identify damages. It is defined by Chan et al. [1], as the use of an on-structure sensing system to monitor structural performance and to evaluate the symptoms of anomalies, deterioration or damages that may affect the operation, serviceability, or safety reliability of a structure.

Traditionally, damage in civil structures was often assessed by visual inspection or Non-Destructive Testing (NDT) methods such as those using X-rays and ultrasonic waves to measure cracks and permanent deformations [2]. Kaphle et al. [3] studied the acoustic emission method to locate the damage in plate-like structures. Major drawbacks of these NDT methods are that the damaged region might not be readily accessible, and the collected data may not be enough for effective prediction of the remaining life of a structure. This has led to the development of methods that examine changes in the vibration characteristics of the structure [1]. Vibration Based Damage Identification

(VBDI) methods have effectively addressed the drawbacks of traditional methods. Many VBDI methods basically rely on measuring the vibration properties such as natural frequencies and mode shapes. The collected data is analyzed which can then be used solely or along with the numerical model of the structure to detect and locate damage.

Initially, implementation and operation of VBDI techniques have been mainly in aircraft structures, railway systems and other machinery [4]. In the past decades, civil engineers have made great effort to detect damage in civil structures. Most of the existing studies on vibration based damage detection were verified by numerical or non-in-situ experimental simulations. Generally, the performance of a damage indicator or a damage identification technique varies with different types of structures. Structures that received the greatest research interest include beams [5, 6], plate elements [7, 8], trusses [9-11], offshore platforms [12-14], steel frames [15-17] and bridges [18-20].

Despite many successful applications in these structures in the recent years, damage detection in complex structures such as buildings, especially asymmetric buildings, remains a challenging task for structural engineers. An asymmetric building can be defined as one in which there is either geometric, stiffness or mass eccentricity. Such buildings exhibit complex vibrations as there is coupling between the lateral and torsional components of vibration, and are referred to as torsionally coupled buildings. As a result of coupled lateral-torsional motions, the lateral forces experienced by various resisting elements (such as columns and walls, etc.) will differ from those experienced by the same elements if the building was symmetric and responded only to planar vibrations [21]. In a separate study the present authors found that, due to torsional coupling, the effect of damage in a beam element has a tendency to influence the other beam elements connected to it. This tendency is different to what occurs in symmetric buildings in which damage in a beam does not influence the other beams in the vicinity. Such a feature was also evident with columns in an asymmetric building. Probably due to their complex behavior, considerably less work is reported in the literature on detecting and locating damage specific to torsionally coupled asymmetric buildings. It is therefore timely to address the problem of detecting and locating damage in such common but rather complicated building structures.

Natural frequency change as the basic feature for damage detection is one of the most common approaches. It can be easily measured from just a few accessible points and it is less contaminated by experimental noise [22]. However changes in frequencies are unable to provide spatial information and hence damage detection methods relying solely on change in natural frequency may not be sufficient for locating damage [23]. The advantage of using mode shapes compared with natural frequencies is that mode shapes contain spatial information and are less sensitive to environmental effects. West [24] presented a systematic use of information on mode shapes to locate structural damage. The research utilized Modal Assurance Criterion (MAC) to determine the level of correlation between modes. However MAC method heavily depends on the completeness of the measured degrees of freedom. Ko et al. [25] presented a method that combined MAC and Coordinate Modal Assurance Criterion (CoMAC) to assess structural damage in steel-framed structures. This study showed that CoMAC analysis could provide more reliable damage localization results. Although mode shape based methods contain spatial information, it is hard to capture accurate and reliable mode shapes with a limited number

of sensors for large structures, especially if higher modes are deemed more favorable than the lower modes for damage detection [26].

Methods based on dynamically measured flexibility have also received considerable attention from many researchers. The motivation of using this method is that the complete vibration parameters for damage detection are not required [27]. Wang et al. [28] performed a sensitivity analysis of Modal Flexibility (MF) on simulated damage of Tsing Ma Bridge. Recently, Sung et al. [29] presents an approach based on the MF matrix to detect damage in cantilever beam-type structures. The proposed approach was successfully validated through a series of numerical and experimental studies on a 10-storey building model for single and multiple damages. The literature confirms that MF based method has a wide variety of applications in damage detection studies, however there is no application in detecting and locating damage in large scale asymmetric building structures.

Modal Strain Energy (MSE) based method was first developed by Stubbs et al. [30], [31]. This method has been used in further studies by Law et al. [11] to detect and locate damage in structures with incomplete and noisy measured modal data. Shi et al. [32] proposed a damage localization technique using the MSE Change Ratio (MSECR). This method only requires mode shapes and the elemental stiffness matrix. The application of the proposed method to a truss structure and a two-storey frame structure demonstrated the capability of this method in locating single and multiple damages. Shih et al. [20] proposed a multi-criteria approach incorporating MF and MSE based methods for detecting damages in slab-on-girder bridges. It was found that for single damage both flexibility and strain energy changes provided accurate results for locating damage. However for multiple damage cases, only the MSE based method was capable of accurately locating the damage.

From the review of the many approaches above, it is evident that the MF change and MSE change methods show better capability to detect and locate damage. Moreover, the overall review of the literature indicated that it is unrealistic to expect damage to be reliably detected, in all cases, by using a single damage index especially in multiple damages scenarios. Combined methods have provided a better chance of structural damage detection. It is believed, that the multi-damage detection of complex asymmetric buildings, treated in this paper, could be achieved by using a Multi-Criteria Approach (MCA) incorporating a combination of MF change and MSE change based methods.

2. Method

2.1 Modified Modal Flexibility method (MMF)

Modal flexibility, F_h of an intact linear (one dimensional) structure can be obtained as [33]

$$F_h = \left[\sum_{i=1}^{n} \frac{1}{\omega_i^2} \phi_i \phi_i^T\right]_h \tag{1}$$

where *i* and *n* are the mode number and total number of modes considered respectively, ϕ_i is the i^{th} mode shape, $\frac{1}{\omega^2}$ is the reciprocal of the square of natural frequencies.

Evaluation of changes in the flexibility matrix of a structure was first proposed by Pandey and Biswas [27] as

$$MFC = F_d - F_h = \left[\sum_{i=1}^{n} \frac{1}{\omega_i^2} \phi_i \phi_i^T\right]_d - \left[\sum_{i=1}^{n} \frac{1}{\omega_i^2} \phi_i \phi_i^T\right]_h \tag{2}$$

where F_h and F_d are MF matrices of the healthy and damaged structure respectively. The maximum absolute value in each column of the MF matrix corresponding to a specific node in the structure is then extracted and written as

$$\overline{\delta_j} = max_j \left|\delta_{kj}\right| \tag{3}$$

where δ_{kj} is element of MFC. $\overline{\delta_j}$ is set as a indicator to measure the change of flexibility for each measurement location.

Wickramasinghe et al. [34] improved this method for detecting damage in suspension bridges by normalize the MFC by F_h as

$$MFC\% = \frac{MFC}{F^h} \times 100\% = \frac{\left[\sum_{i=1}^{n} \frac{1}{\omega_i^2} \phi_i \phi_i^T\right]_d - \left[\sum_{i=1}^{n} \frac{1}{\omega_i^2} \phi_i \phi_i^T\right]_h}{\left[\sum_{i=1}^{n} \frac{1}{\omega_i^2} \phi_i \phi_i^T\right]_h} \tag{4}$$

For a three dimensional asymmetric building each node in a member of the structure contains 3 translational degrees of freedom (DOFs). In order to apply MF based method to asymmetric buildings the MF matrix $MFC(2L + V)$ of j measurement locations will then be $3j \times 3j$ array instead of $j \times j$. where L and V denote the lateral and vertical components of the mode shapes. The modified $MFC\%$ can then be expressed as

$$\overline{\delta}\%(2L + V)_j = max(max_{(3j-2)}\left|\delta\%_{k(3j-2)}\right| \ : \ max_{(3j)}\left|\delta\%_{k(3j)}\right|) \tag{5}$$

Reconstructing the Eq. (4) in matrix notation

$$MMF\%_i = \begin{bmatrix} \delta\%_{11} & \delta\%_{12} & \delta\%_{13} & \cdots & \delta\%_{1(3j-2)} & \delta\%_{1(3j-1)} & \delta\%_{1(3j)} \\ \delta\%_{21} & \delta\%_{22} & \delta\%_{23} & \cdots & \delta\%_{2(3j-2)} & \delta\%_{2(3j-1)} & \delta\%_{2(3j)} \\ \delta\%_{31} & \delta\%_{32} & \delta\%_{33} & \cdots & \delta\%_{3(3j-2)} & \delta\%_{3(3j-1)} & \delta\%_{3(3j)} \\ \vdots & \vdots & \vdots & \ddots & \vdots & \vdots & \vdots \\ \delta\%_{(k-2)1} & \delta\%_{(k-2)2} & \delta\%_{(k-2)3} & \cdots & \delta\%_{(k-2)(j-2)} & \delta\%_{(k-2)(3j-1)} & \delta\%_{(k-2)(3j)} \\ \delta\%_{(k-1)1} & \delta\%_{(k-1)2} & \delta\%_{(k-1)3} & \cdots & \delta\%_{(k-1)(j-2)} & \delta\%_{(k-1)(3j-1)} & \delta\%_{(k-1)(3j)} \\ \delta\%_{k1} & \delta\%_{k2} & \delta\%_{k3} & \cdots & \delta\%_{k(j-2)} & \delta\%_{k(3j-1)} & \delta\%_{k(3j)} \end{bmatrix}_{3j \times 3j} \tag{6}$$

Taking the maximum absolute value from each column then we have

$$max_j\left|\delta\%_{kj}\right| = [max|\delta\%_{k1}| \ max|\delta\%_{k2}| \ max|\delta\%_{k3}| \ \cdot\cdot \cdot \ max\left|\delta\%_{k(3j-2)}\right| \ max\left|\delta\%_{k(3j-1)}\right| \ max\left|\delta\%_{k(3j)}\right|]_{1\times 3j} \tag{7}$$

By considering the 3 DOFs of each node we take the maximum absolute value from every three $\delta\%_j$ in the row

$$\overline{\delta}\%(2L+V)_j = [max(max|\delta\%_{k1}|, max|\delta\%_{k2}|, max|\delta\%_{k3}|)_1 \cdot\cdot \\ \cdot \ max(max|\delta\%_{k(3j-2)}|, max|\delta\%_{k(3j-1)}|, max|\delta\%_{k(3j)}|)_j]_{1\times j} \tag{8}$$

2.2 Modified Modal Strain Energy method (MMSE)

In this paper, the previous MSE based method proposed by Stubbs et al. [30] has been enhanced in order to apply to asymmetric building structures. For a linear, intact structure with N_e elements, the i^{th} modal strain energy of a structure is given by

$$U_i = \Phi_i^T K \Phi_i \tag{9}$$

Where K is the system stiffness matrix which assembles all element stiffness matrices, and Φ_i is the i^{th} intact mode shape. Modal strain energy U_{ij} of the j^{th} element is defined as

$$U_{ij} = \Phi_i^T K_j \Phi_i \tag{10}$$

where K_j is the element stiffness matrix. For the i^{th} mode, the fraction of MSE is concentrated in the j^{th} member is given by

$$f_{ij} = \frac{U_{ij}}{U_i} \tag{11}$$

The damage in this study is assumed to effectively reduce the Young's modulus in material, so K_j could be written as

$$K_j = E_j K_{j0} \tag{12}$$

where E_j is parameter representing the Young's modulus of j^{th} element, and the matrix K_{j0} contains only geometric quantities. Similarly, for a damaged structure we have

$$U_i^d = \Phi_i^{dT} K^d \Phi_i^d \tag{13}$$

$$U_{ij}^d = \Phi_i^{dT} K_j^d \Phi_i^d \tag{14}$$

$$f_{ij}^d = \frac{U_{ij}^d}{U_i^d} \tag{15}$$

$$K_j^d = E_j^d K_{j0} \tag{16}$$

Stubbs and Kim [31] state that when number of element N_e is large, both f_{ij} and f_{ij}^d tend to be much less than unity. It gives

$$\frac{(f_{ij}^d + 1)}{(f_{ij} + 1)} = 1 \tag{17}$$

Substituting Eqs. (11) and (15) into Eq. (17) yields

$$\frac{(U_{ij}^d + U_i^d)U_i}{(U_{ij} + U_i)U_i^d} = 1 \tag{18}$$

Substituting Eqs. (9), (10), (13) and (14) into Eq. (18) and rearranging we obtain

$$\frac{E_j^d}{E_j}\frac{[\Phi_i^{dT}K_{j0}\Phi_i^d+\left(\frac{1}{E_j^d}\right)\Phi_i^{dT}K^d\Phi_i^d]U_i}{[\Phi_i^TK_{j0}\Phi_i+\left(\frac{1}{E_j}\right)\Phi_i^TK\Phi_i]\,U_i^d}=1 \tag{19}$$

The damage localization indicator β_{ij} can be defined to be the ratio of intact material strength and damaged material strength E_j/E_j^d and imposing the approximations $K\approx E_jK_0$ and $K^d\approx E_j^dK_0$, we obtains

$$\beta_{ij}=\frac{E_j}{E_j^d}=\frac{(\Phi_i^{dT}K_{j0}\Phi_i^d+\Phi_i^{dT}K_0\Phi_i^d)\Phi_i^TK\Phi_i}{(\Phi_i^TK_{j0}\Phi_i+\Phi_i^TK_0\Phi_i)\Phi_i^{dT}K\Phi_i^d} \tag{20}$$

When take modes of interest (Nm) into consideration, the following formation can be used

$$\beta_j=\frac{\sum_{i=1}^{Nm}\{(\Phi_i^{dT}K_{j0}\Phi_i^d+\Phi_i^{dT}K_0\Phi_i^d)\Phi_i^TK\Phi_i\}}{\sum_{i=1}^{Nm}\{(\Phi_i^TK_{j0}\Phi_i+\Phi_i^TK_0\Phi_i)\Phi_i^{dT}K\Phi_i^d\}} \tag{21}$$

For a more robust damage detection criterion, the normalized indicator is given by

$$Z_j=\frac{\beta_j-\bar{\beta}}{\sigma_\beta} \tag{22}$$

It is found that Stubbs' damage index is only helpful when the damage is in vertical the members. However, structural members of an asymmetric frame structure predominantly have two types of elements (1) horizontal members (beams) and (2) vertical members (columns). Normally vibration modes of a building structure are mainly horizontal instead of vertical; in this case MSE change in the vertical members would be dominated by the lateral MSE. On the other hand, MSE change of the horizontal members would be contributed significantly by the vertical MSE [14]. Therefore in this study two damage indicators, a lateral damage indicator and a vertical damage indicator, are formulated by decomposing Stubbs' damage index. The modified damage indicator could rewritten as

$$\beta_j^L=\frac{\sum_{i=1}^{Nm}\{(\Phi_i^{LdT}K_{j0}\Phi_i^{Ld}+\Phi_i^{LdT}K_0\Phi_i^{Ld})\Phi_i^{LT}K\Phi_i^L\}}{\sum_{i=1}^{Nm}\{(\Phi_i^{LT}K_{j0}\Phi_i^L+\Phi_i^{LT}K_0\Phi_i^L)\Phi_i^{LdT}K\Phi_i^{Ld}\}} \tag{23}$$

$$\beta_j^L=\frac{\sum_{i=1}^{Nm}\{(\Phi_i^{VdT}K_{j0}\Phi_i^{Vd}+\Phi_i^{VdT}K_0\Phi_i^{Vd})\Phi_i^{VT}K\Phi_i^V\}}{\sum_{i=1}^{Nm}\{(\Phi_i^{VT}K_{j0}\Phi_i^V+\Phi_i^{VT}K_0\Phi_i^V)\Phi_i^{VdT}K\Phi_i^{Vd}\}} \tag{24}$$

Then the modified normalized indicator is defined as

$$Z_j^L=\frac{\beta_j^L-\overline{\beta^L}}{\sigma_{\beta^L}} \tag{25}$$

$$Z_j^V=\frac{\beta_j^V-\overline{\beta^V}}{\sigma_{\beta^V}} \tag{26}$$

3. Application

3.1 Validation of modelling techniques

Before applying the developed technique to detect damage in an asymmetric building, the modelling techniques will be validated by comparing results with those from experimental testing. Towards this end, a laboratory model of an asymmetric building was designed and constructed as shown in Figure 1(a). It was designed in such a way that some of the earlier modes were 3 dimensional modes with torsional coupling. The upper floor of the model is made of a right triangular steel plate with dimensions 400mm x 200mm and thickness 3mm supported at each of its 3 corners by a column which is a plain bar of 8mm diameter. The dimensions of lower floor are 800mm in length and 400mm in width, the thickness of the steel plate is 1mm and is supported by 9 plain bars of 8mm in diameter. At the time the test specimen was designed, a corresponding finite element model of the specimen was developed in ANSYS [35]. The general modelling scheme for the structure is depicted in Figure 1(b). The details of the structure are listed in Table 1. It is assumed that there is full connection between the slabs and columns.

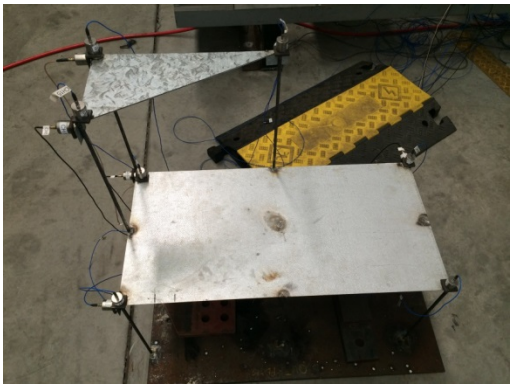

(a) Test Specimen

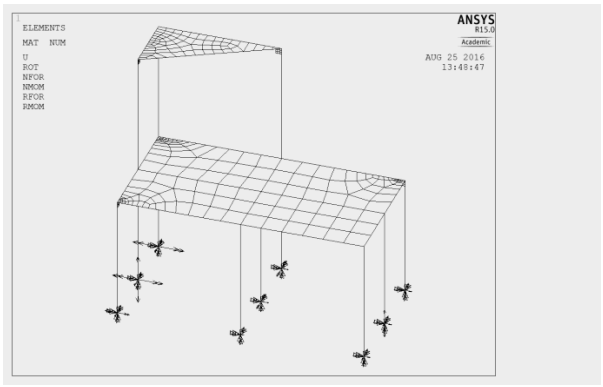

(b) FE model of test specimen

Figure 1 Laboratory model with attached with sensors

Table 1 Geometric and material properties for the test specimen

Flexural member	Slab (1st floor)	Slab (2nd floor)	Column (all)
Element type	Shell 181	Shell 181	Beam 188
Material	Steel	Steel	Steel
Length	800 mm	400 mm	400 mm
Width	400 mm	200 mm	-
Depth	1 mm	3 mm	-
Diameter	-	-	8 mm
Poisson's ratio	0.3	0.3	0.3
Density	7850 kg/m^3	7850 kg/m^3	7850 kg/m^3
Modulus of elasticity	200 GPa	200 GPa	200 GPa

Prior to the free vibration testing, the data acquisition system was established; which included 13 single-axis PCB® 393B05 integrated circuit piezoelectric accelerometers as shown in Figure 2, positioned to measure vertical and lateral accelerations. All sensors were self-calibrated; this means after a small period the sensors are able to automatically pickup correct acceleration without further calibrations. The sensors are able to measure a signal in the frequency range between 0.7 Hz to 450 Hz (±5%) with sensitivity of 10V/m/s2 (±10%). They are attached to the test specimen using the N42 Rare Earth Magnets. The other instruments used in the modal testing are also shown in Figure 2. The experimental vibration system consists of three main components; (i) impact hammer (ii) accelerometers and (iii) data acquisition system. The impact hammer is used to provide a source of excitation to the test specimen. The accelerometers are used to convert the mechanical motion of the structure into an electrical signal. The Software "SignalExpress" is used to execute signal processing and the Operational Modal Analysis (OMA) software "ARTeMIS is then used to process the modal analysis.

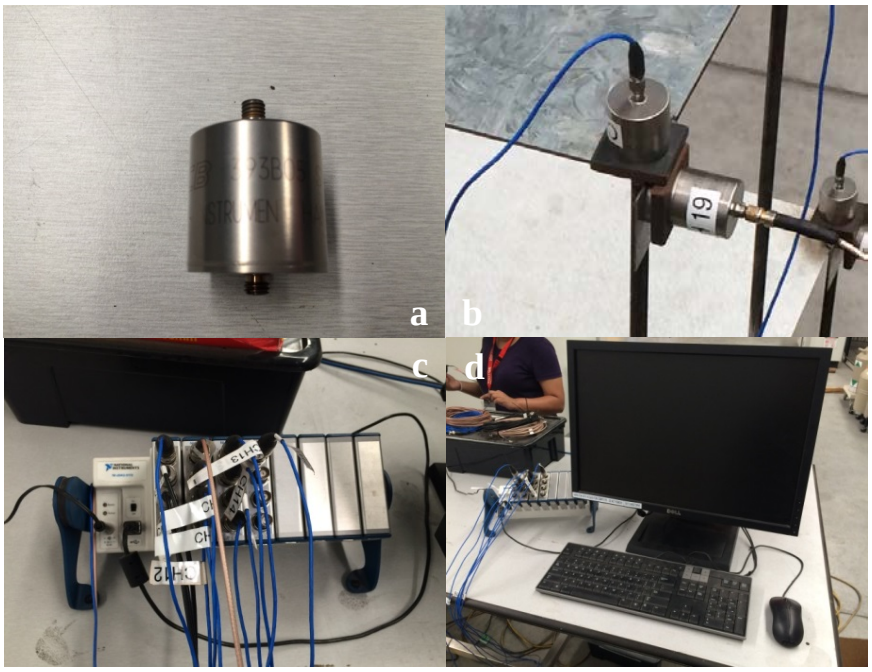

Figure 2 Operational Model Testing Instruments: (a) accelerometers; (b) accelerometers mounted on structure; (c) NI cDAQ modules; (d) computer used to proceed data

The free vibration test was conducted in the undamaged state of the structure which is considered as the baseline structure. The 2nd and 3rd dynamic tests were conducted at the damaged states with damage extents of 10% and 40% reductions in stiffness (obtained by reducing the diameter across a length of 100mm since stiffness is proportional to cross section of the element) in the cross-section of the 9th column element (to enhance the validation of the FE model) as shown in Figure 3. The free vibration measurement is an output data-only dynamic testing where the wind and human activities are used as natural ambient excitations. Since the specimen was placed in the laboratory and not subjected to any ambient loading, artificial excitation was adopted. In an effort to excite the structure, random tapping was provided through an impact hammer made of foam (to reduce the

negative impact). All the acceleration data was captured in the time domain by the DAQ system while conducting the experiment and was then transferred to the ARTeMIS modal analysis software to obtain modal parameters.

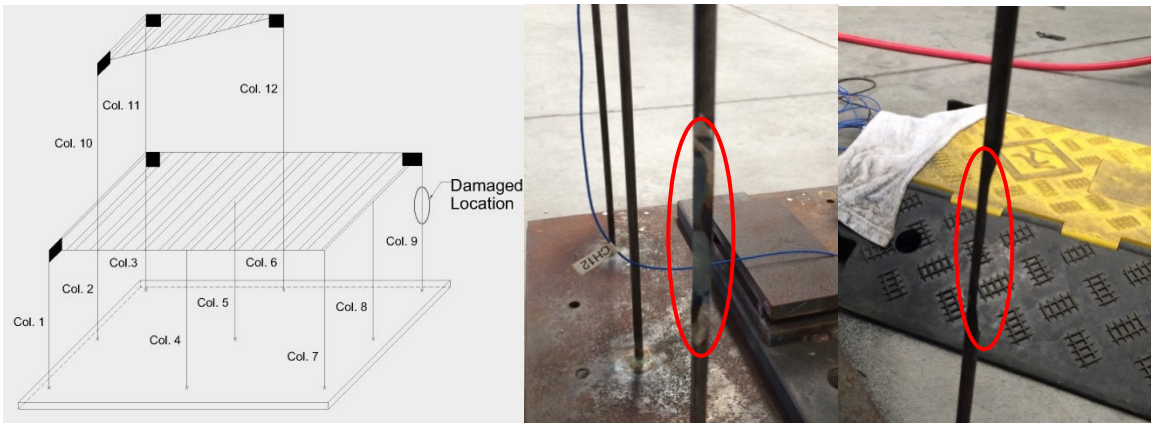

Figure 3 Flaw at steel bar of the model

The natural frequencies and mode shapes were determined by SSI-DATA (UPC) in ARTeMIS modal analysis software. A comparison between numerical and experimental dynamic characteristics was conducted and presented in Table 2. Model updating was done to tune in the structural parameters of the FE model such that natural frequencies obtained in the experiment and FE model closely match. With the change of structural parameters such as connectivity of structural elements, support conditions and Young's Modulus, the initial FE model was updated to match the measured natural frequencies as close as possible. The comparison of natural frequencies of the test model and those obtained from FE analysis is done by calculating the relative error $f_{error} = \frac{(f_{exp} - f_{fem})}{f_{exp}} \times 100$, where f_{exp} is natural frequency obtained in the experiment and f_{fem} is the corresponding natural frequency obtained in the FE analysis.

Table 2Correlation between experimental and FE model

Mode	Undamaged			10% damaged			40% damaged		
	Natural Frequency (Hz)		f_{error} (%)	Natural Frequency (Hz)		f_{error} (%)	Natural Frequency (Hz)		f_{error} (%)
	f_{exp}	f_{fem}		f_{exp}	f_{fem}		f_{exp}	f_{fem}	
1	6.418	6.4087	0.14	6.406	6.3989	0.11	6.37	6.3602	0.15
2	6.869	6.8127	0.82	6.881	6.8065	1.08	6.848	6.7825	0.96
3	12.426	12.783	-2.87	12.346	12.748	-3.26	12.125	12.604	-3.95
4	17.535	17.972	-2.49	17.491	17.959	-2.68	17.416	17.893	-2.74
5	19.645	19.865	-1.12	19.614	19.858	-1.24	19.601	19.812	-1.08

The differences between the measured and computed natural frequencies of the test specimen are smaller than 4%, which demonstrates a very good correlation of results. It is hence evident from Table 2 that the natural frequencies obtained from the experiment and

FE analysis compare reasonably well. Graphical representation of the captured experimental mode shapes of the structure in its undamaged state is illustrated in Figures 4. The modes obtained from the FE analysis are presented in Figures 5. In addition, mode shapes were also compared by calculating MAC values, which vary from 0 to 1, with 0 for no correlation and 1 for full correlation. It can be seen from Figure 4 and Table 3 that the 2 sets of mode shapes compare reasonably well. It is hence concluded that the measured and computed natural frequencies and mode shapes are in good agreement and provide confidence in the modelling techniques used in this study.

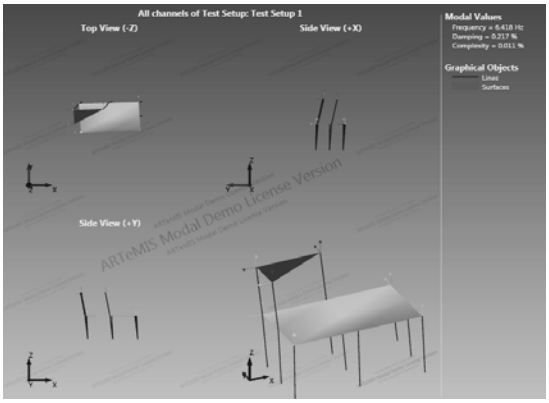

(a) Mode 1, f_1 = 6.418 (laboratory model)

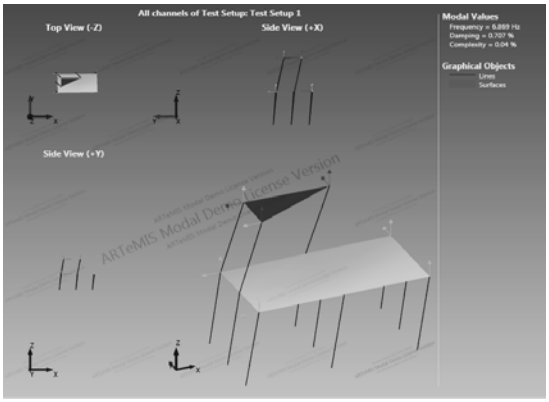

(b) Mode 2, f_2 = 6.869 (laboratory model)

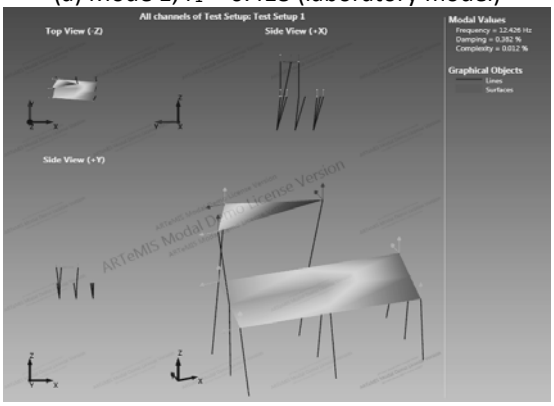

(c) Mode 3, f_3 = 12.426 (laboratory model)

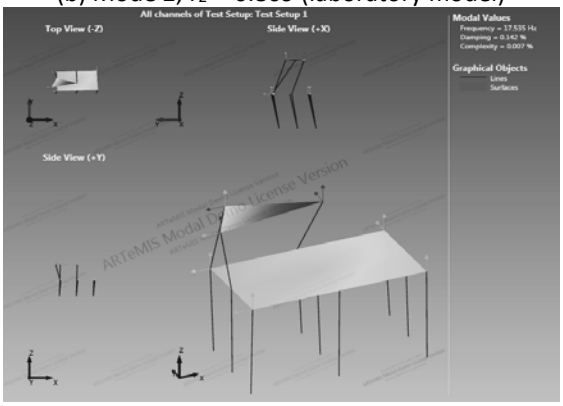

(d) Mode 4, f_4 = 17.535 (laboratory model)

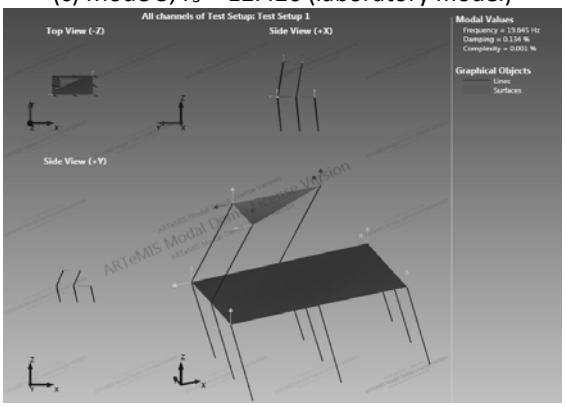

(e) Mode 5, f_5 = 19.645 (laboratory model)

Figure 4 Experimentally obtained vibration modes of undamaged model

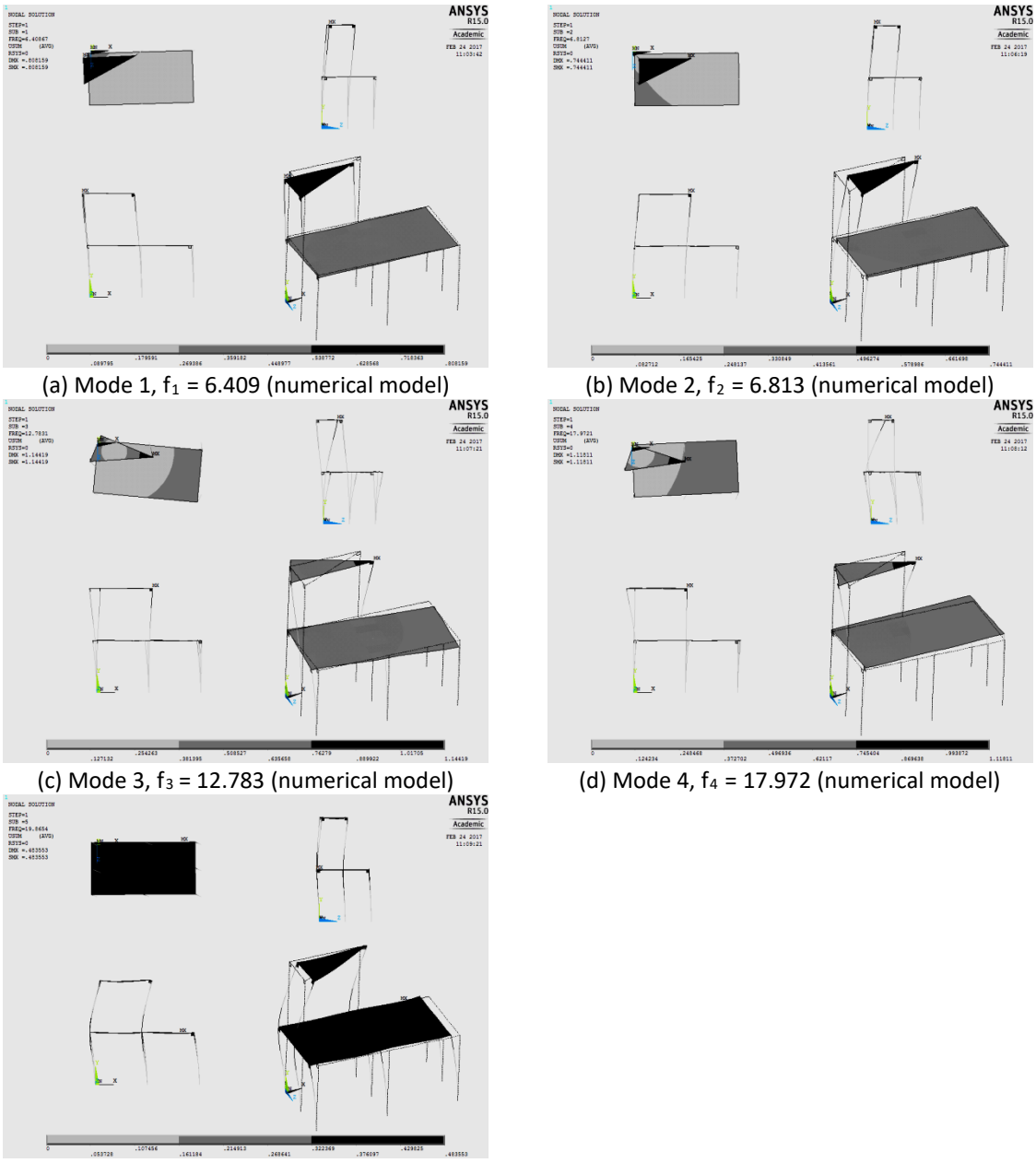

(a) Mode 1, f_1 = 6.409 (numerical model)

(b) Mode 2, f_2 = 6.813 (numerical model)

(c) Mode 3, f_3 = 12.783 (numerical model)

(d) Mode 4, f_4 = 17.972 (numerical model)

(e) Mode 5, f_5 = 19.865 (numerical model)

Figure 5 Modal analysis results of first 5 modes using ANSYS Mechanics AODL

To confirm the feasibility of using the two selected damage indices to detect damage, the measured natural frequencies and associated mode shapes obtained from the free vibration testing of both the intact and damaged test models under 2 damage scenarios, are used to calculate the MMF and MMSE based damage indices. These are plotted in Figures 6, and it is evident that there is a distinct peak in each of these figures corresponding to the position of the damaged element. These results conform well to the damage scenario. Even though only three modes obtained from the experimental testing were used to evaluate the damage detection parameters, they are able to predict the damage location reasonably well. This establishes that both the chosen damage indices MMF and MMSE are competent in locating damage in the test structure and provide

further confidence in damage detection in asymmetric building structures using the proposed procedure.

Table 3 MAC values comparing experimental and analytical data

Undamaged model		Analytical data				
		Mode 1	Mode 2	Mode 3	Mode 4	Mode 5
Experimental data	Mode 1	0.9820	0.9559	0.5441	0.3537	0.5006
	Mode 2	0.9346	0.9974	0.7180	0.5214	0.5780
	Mode 3	0.3443	0.5377	0.8931	0.8456	0.4004
	Mode 4	0.4474	0.6152	0.7967	0.9325	0.3261
	Mode 5	0.4297	0.5052	0.3620	0.3260	0.9902

The validation of the modelling techniques by comparison of the experimental and computed results for frequencies, mode shapes and MAC values for both the healthy and the damaged building models and the establishment of the feasibility of the chosen damage detection indices (as described earlier) provide adequate confidence in the procedure used in this paper for damage detection in asymmetric buildings.

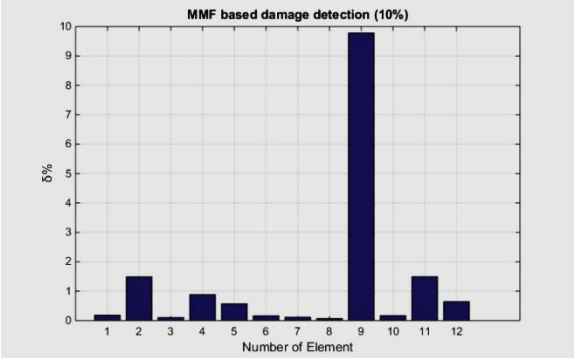

(a) Result of MMF with 10% section reduction

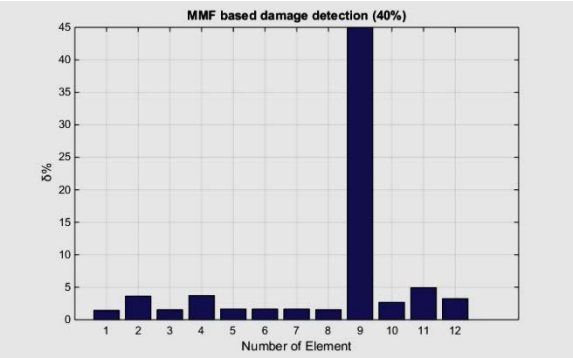

(b) Result of MMF with 10% section reduction

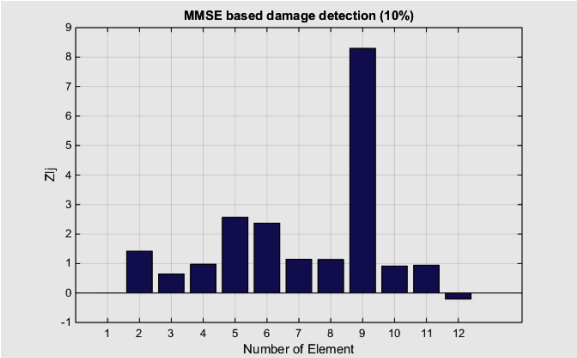

(c) Result of MMSE with 10% section reduction

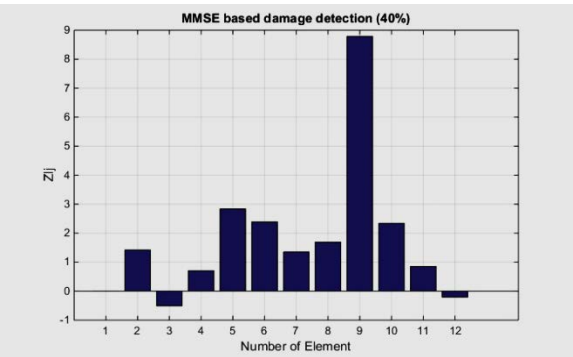

(d) Result of MMSE with 40% section reduction

Figure 6 Result of experimental test specimen

3.2 Numerical example

To illustrate the procedure a full scale ten storey L-shape asymmetric building structure is designed and generated using Finite Element (FE) software ANSYS [35]. This is used to evaluate the performance of the proposed MCA which incorporates MMF change ratio $\overline{\delta}\%$ and MMSE based damage indices Z_j^L and Z_j^V. The FE model of the asymmetric structure consists of 140 column elements (1200mm*500mm), 190 beam elements (600mm*400mm) and 164 nodes. The general modelling scheme for the structure is depicted in Figure 7. The geometric and material properties of the building are listed in Table 4.

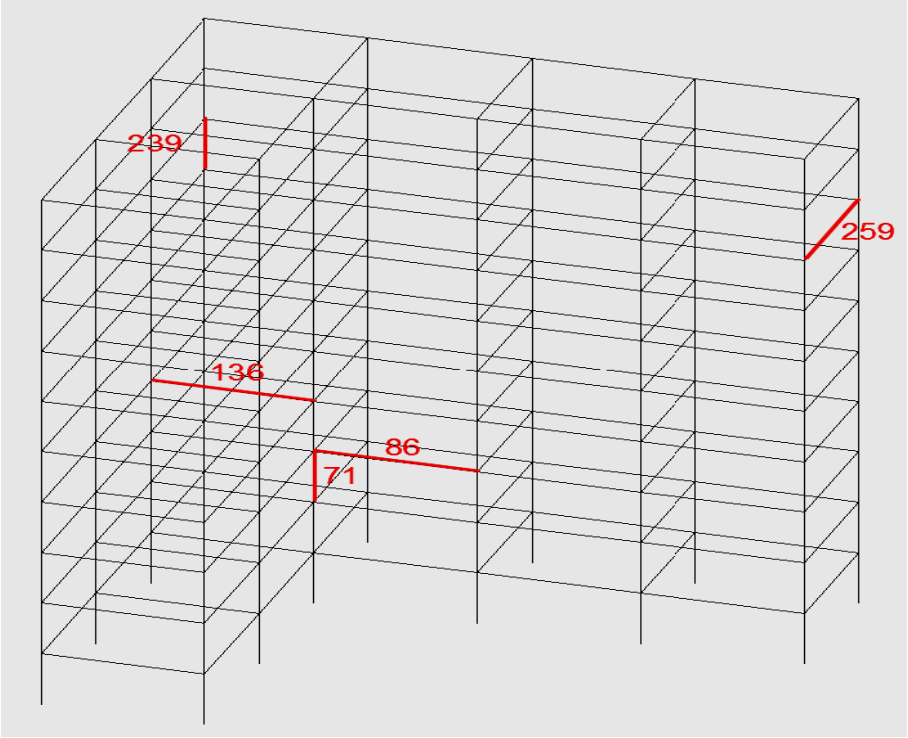

Figure 7 Numerical model and induced damage members

Table 4 Geometric and material properties for FE model

Member	Beam (all)	Column (all)
Element type	Beam 188	Beam 188
Material	RC	RC
Length (mm)	8000	4000
Width (mm)	400	500
Depth (mm)	600	1200
Poisson's ratio	0.3	0.3
Density (kg/m^3)	2427	2427
Modulus of elasticity (GPa)	42	42

To demonstrate the versatility of the technique developed and presented above, five different damage scenarios have been applied in this ten storey asymmetric frame

structure as shown in Table 5. Elements associated with single damage locations having 30% loss of Young's modulus across the full length of the column or the beam are first considered to examine the capability of the proposed method to detect damage in both beam and column type of elements. The other three damage scenarios considered multiple damage locations with either damage in both a column and a beam, multi beam damages or multi column damages to check if there is any interaction between a damaged element and the elements in its vicinity. The different extents of damage in multi damage scenario were designed to examine the capability of the proposed method in the presence of mild and sever damage cases.

Table 5 Damage scenarios

Scenarios	Damaged element no.	Damaged node nos.	Stiffness decrease
D1	71 (column)	51 & 52	30%
D2	86 (beam)	59 & 60	30%
D3	136 (beam) & 239 (column)	75,76 & 120,121	30% & 30%
D4	86 (beam) & 259 (beam)	59,60 & 135,136	30% & 10%
D5	71(column) & 239 (column)	51,52 & 120,121	10% & 30%

The basic modal parameters of natural frequencies and mode shapes in both the intact and damaged states of the building are extracted from the results of FE modal analyses. These parameters are then used to calculate the proposed damage indices. The peak values of the plots will then indicate the locations of the simulated damage in the corresponding damage scenarios. The accuracy of the damage detection method is then evaluated through observation of the results.

4. RESULTS AND DISCUSSION

For the present study 20 modes are assumed to be measureable in FE analysis, however in practice there might be only the first few modes that could be measured due to lack of access to sensor locations and limitation of sensors. To illustrate the proposed method in this study only the first five natural frequencies and associated mode shapes obtained from the FE analysis are used to calculate MMF and MMSE. The first five modal frequencies of the intact and damaged structures are listed in Table 6. It is found that modal frequency decreases in all damage scenarios. This agrees with the assumption that damage increases MF of the structures which lead to a decrease in the modal frequency.

Table 6 Natural frequency from FE analysis

Damage Scenario		Mode 1 f_1 (Hz)	Mode 2 f_2 (Hz)	Mode 3 f_3 (Hz)	Mode 4 f_4 (Hz)	Mode 5 f_5 (Hz)
Intact		0.69393	0.79267	0.86986	1.78447	2.22265
Single	D1	0.69391	0.79263	0.86978	1.78445	2.22252
	D2	0.69385	0.79266	0.86984	1.78437	2.22260
Multiple	D3	0.69384	0.79265	0.86975	1.78443	2.22262
	D4	0.69385	0.79263	0.86984	1.78436	2.22260
	D5	0.69391	0.79264	0.86975	1.78446	2.22260

4.1 MMF Method

MMF is calculated by using Equations 14, 15 and 16. The x-axis of the plot shown in Figure 8 represents the number of nodes instead of elements, because it is observed that the nodal coordinates of the structure are shared by the damaged members and the non-damaged members connected to it. So the damage is not only expected to be identifiable at the damaged member itself, but also at the members connected to it [36]. This makes the results more complex when the element numbers are plotted instead of the node numbers.

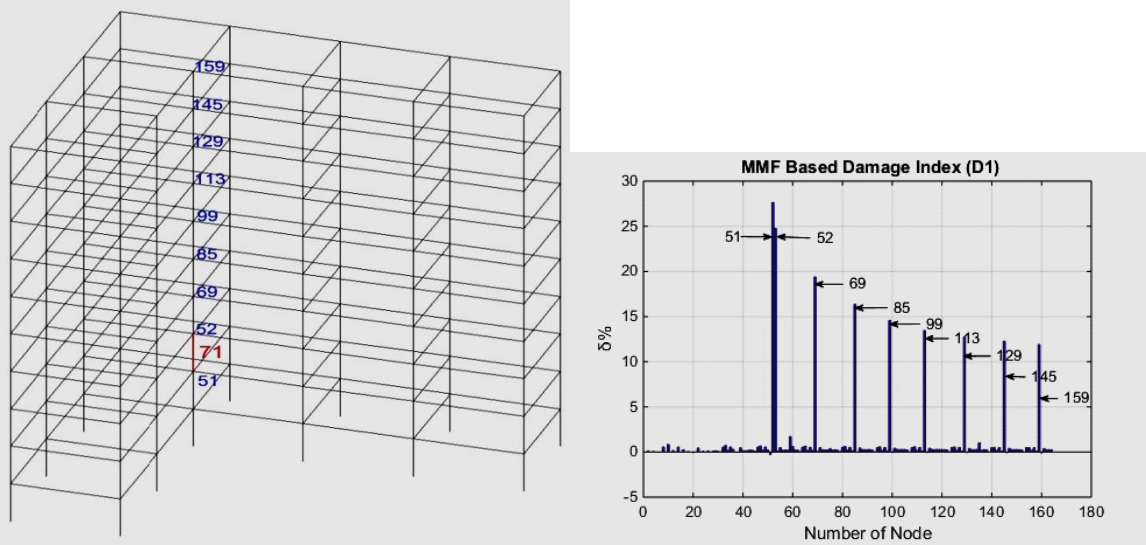

Figure 8 Results of single damage scenario D1 using MMF method

Numerical results for the first damage scenario are shown in Figure 8. Location of the peak of the plot correctly indicates the damage location of the structure. It seems that the columns in the upper floor (with higher node numbers) which connect to the damaged column are affected by the stiffness change. For example, the reduced stiffness (of column element 71, connected by nodes 51 & 52) increases the modal flexibility of the damaged column as well as that of all the columns above. The plots also show that the modal flexibility change ratio of the upper floor columns decrease progressively away from the damaged column.

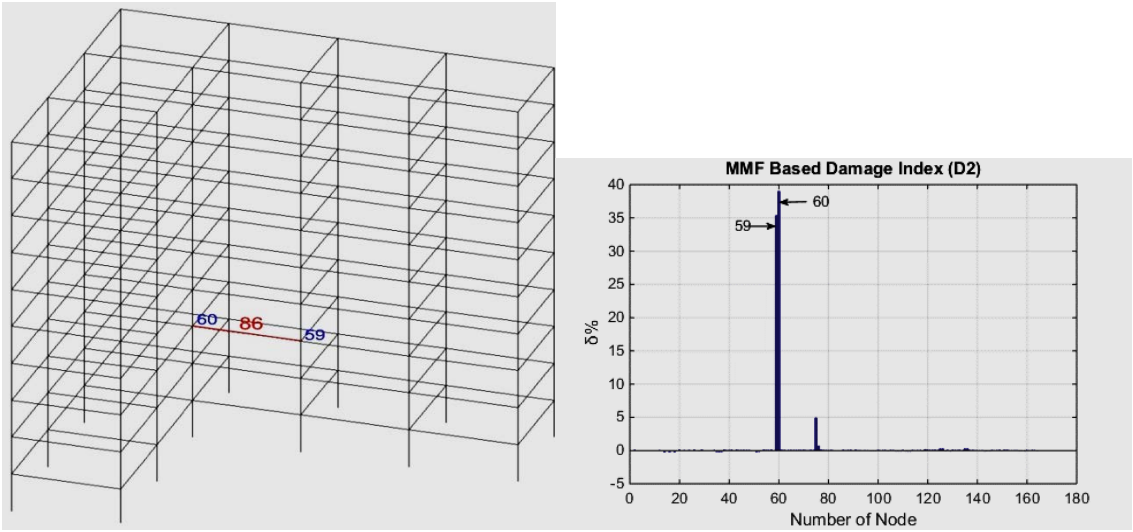

Figure 9 Results of single damage scenario D2 using MMF method

Results of second damage scenario are shown in Figure 9. The peak conforms well this damage scenario. Different to the column damaged case, the damage of the beam element is clearly presented in the plot. These plots convey the information that column damage is more severe and can affect the columns above that level, while beam damage does not propagate elsewhere.

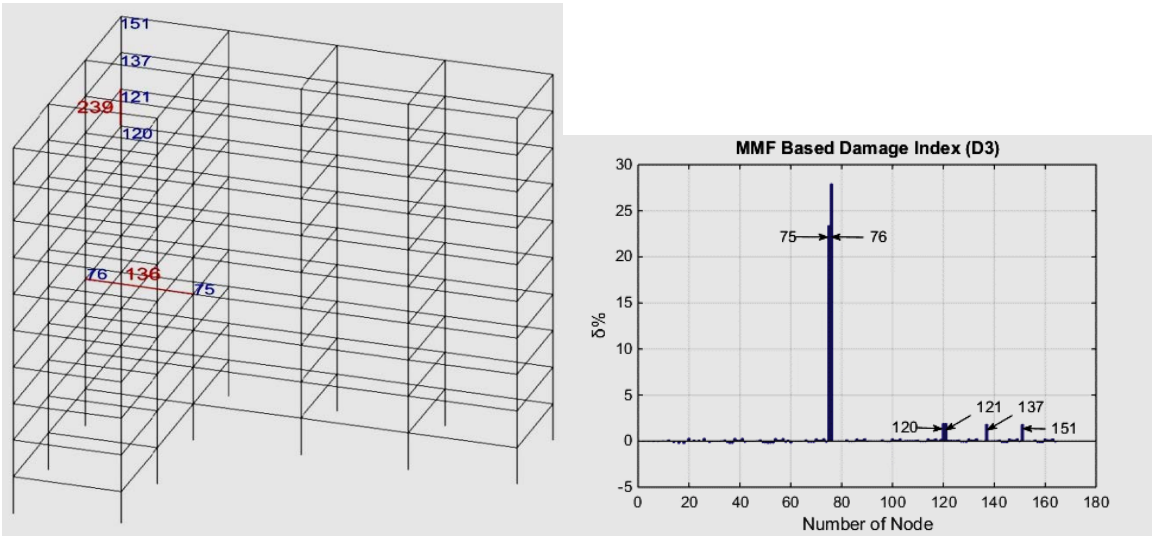

Figure 10 Results of multiple-damage scenario D3 using MMF method

Damage scenarios D3 –D5 are set up to study the damage detection capability of the MMF based DI for multiple damage cases. Figure 10 presents the results of multiple-damage scenario D3. It can be seen that damage in the beam is correctly located by the higher peak. The damage of the column element is shown by the smaller peak. It is again evident that as in damage D1, modal flexibility dose not only increase in the damaged member itself but also the columns connected to it and in the columns above.

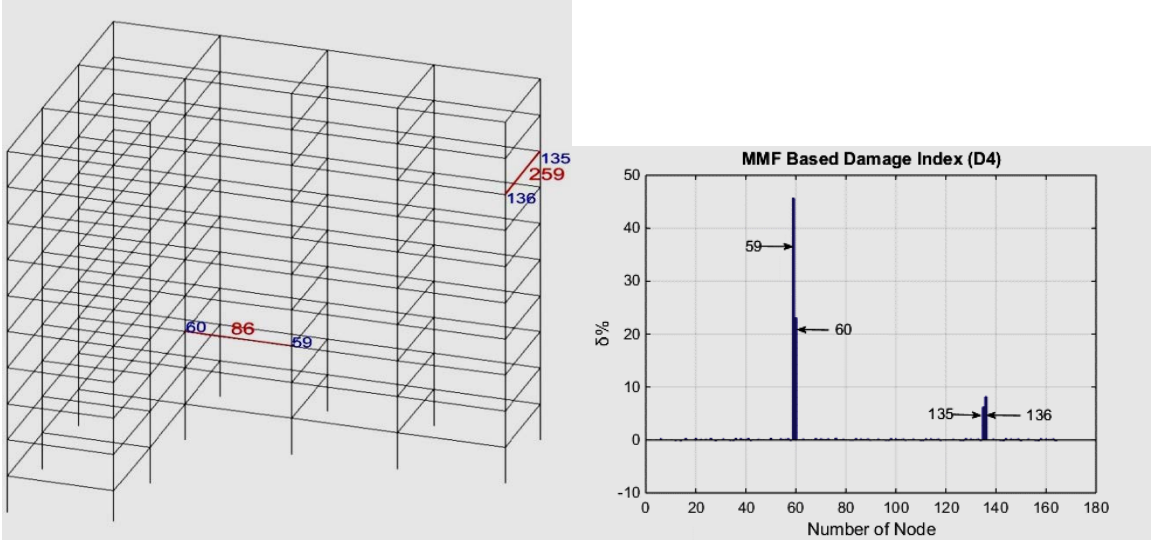

Figure 11 Results of multiple-damage scenario D4 using MMF method

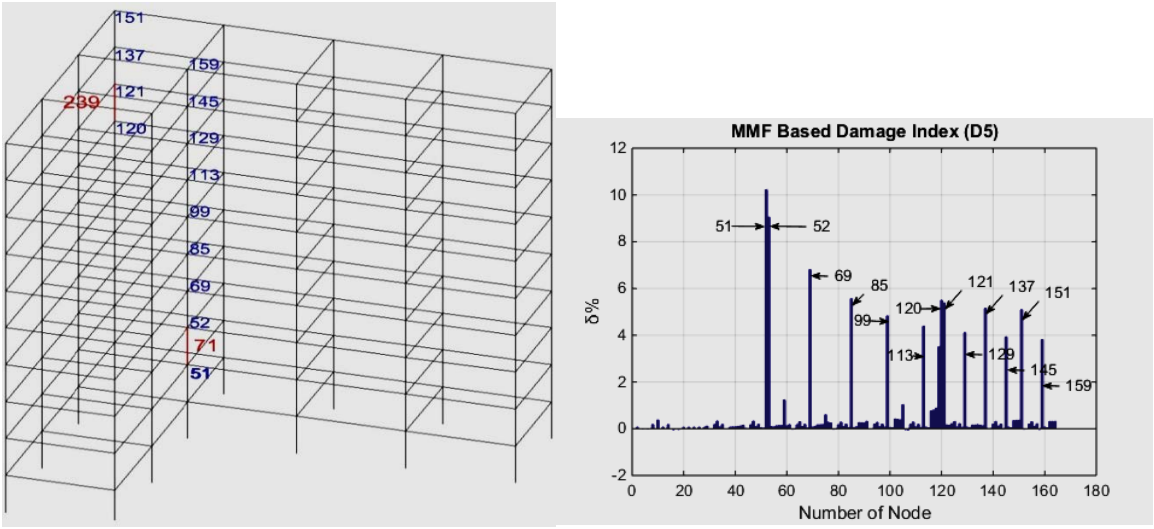

Figure 12 Results of multiple-damage scenario D5 using MMF method

Results of multiple damage scenarios D4 and D5 are presented in Figures 11 and 12. In scenario D4 both damaged elements are beams and are identified by the two distinct peaks. Moreover, damage with a higher severity (in beam "86") is indicated by the higher peak in $\overline{\delta}\%$. Scenario D5 pertains to damage in 2 column elements. Results correctly located both damages, but the severity is not well defined. As before this particular damage index shows peaks corresponding to the columns above the damaged columns, as also observed earlier.

Another feature evident from the results is that damage in a member at a lower level in the building seems to be more severe than that in a member at a higher level in the building, as indicated by the amplitudes of the corresponding peaks. But, more results will be necessary to confirm this trend in a somewhat quantitative manner.

It has been shown above that the MMF method has a good capability of locating beam damage. However, when the damaged member is a column in a multiple damage case,

this damage is unlikely to be identified clearly compared to the damage in a beam element. It was also observed during the analysis that the change between the intact and damaged mode shapes in the vertical components was greater than the change in the horizontal components. This may be because in each floor all the columns are connected by beams and they tend to vibrate as one body. Although the vibration modes under consideration are mainly horizontal instead of vertical, damage in one or two column elements may not be enough to have much influence on the horizontal motion.

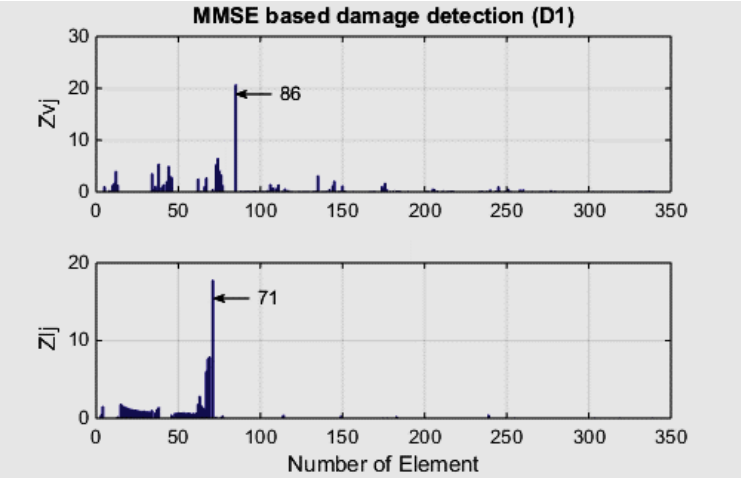

Figure 13 Results of single-damage scenario D1 using MMSE method

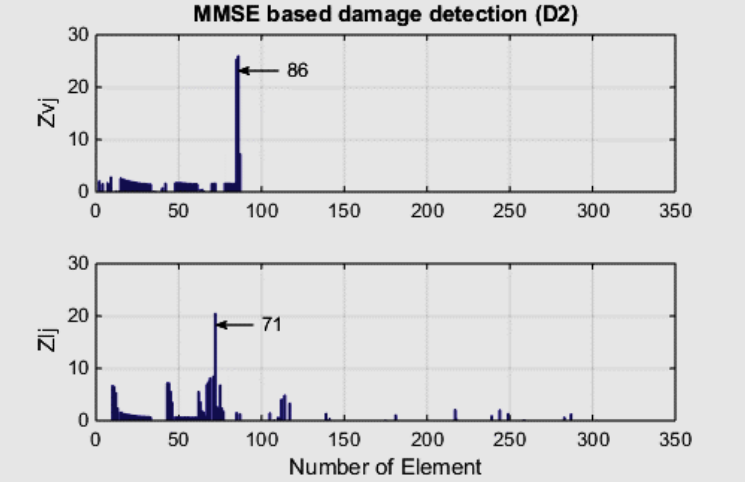

Figure 14 Results of single-damage scenario D2 using MMSE method

4.2 MMSE Method

Figures 13 - 17 show the results of the MMSE method where vertical and horizontal damage indicators have been used in the upper and lower parts of each Figure. In the results of the single column damage scenario in Figure 13, the lateral indicator Z_j^L shows that the damaged member is most likely column 71 and hence correctly located this damage. From the results of the vertical indicator Z_j^V, it is evident that beam element 86 has a peak value which indicates damage. It has to be noted that the beam element 86 is connected to the column element 71. This trend agrees with the previous discussion on

the damage in members having shared nodal coordinates. The results of single beam damage scenario are shown in Figure 14. The peak value of the vertical indicator Z_j^V clearly locates the damaged beam. From these results, it is evident that the MMSE method correctly locates the damaged node as well as the elements connected to it. This is useful information in damage detection strategies.

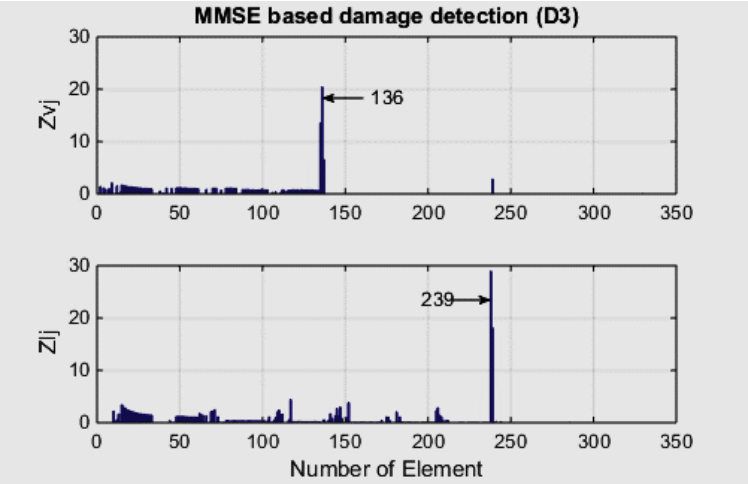

Figure 15 Results of multiple-damage scenario D3 using MMSE method

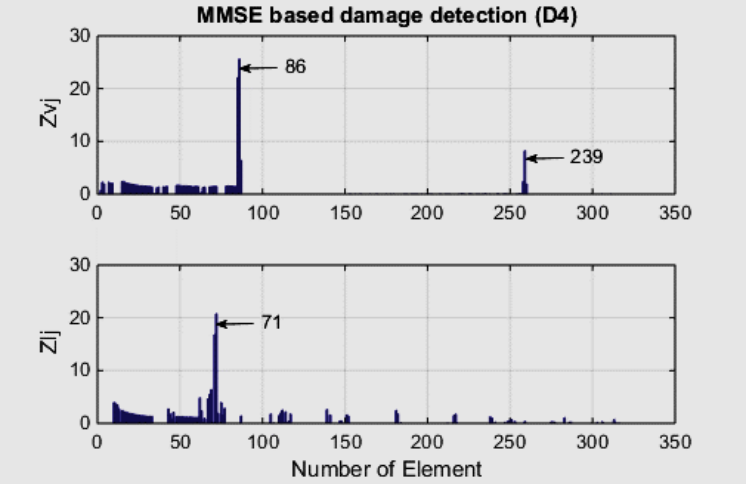

Figure 16 Results of multiple-damage scenario D4 using MMSE method

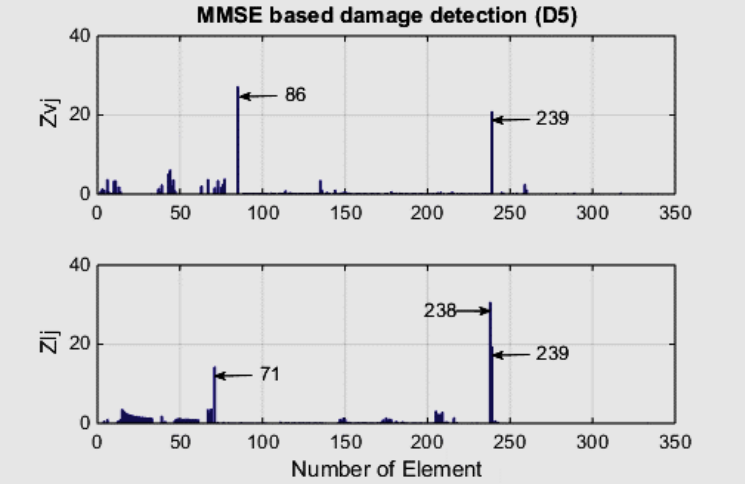

Figure 17 Results of multiple-damage scenario D5 using MMSE method

Damage scenarios D3-D5 investigate the damage detection for multi-damage locations. The damaged elements in D3 consist of a beam element 136 and a column element 239. Figure 15 shows the results of both damage indices. It can be noticed that the peak value of vertical index Z_j^V correctly located the beam damage in element 136, while the peak value of lateral index Z_j^L successfully located the column damage in element 239. The multiple damage scenarios D4 and D5 investigate double beam (elements 86 and 259) damage and double column (element 71 and 239) damage cases, with different damage severities of the two members. The result of damage scenario D4 is presented in Figure 16, the vertical index Z_j^V in this case correctly located both damaged beams as shown by the two distinct peaks. It is also evident that the greater damage severity is indicated by the higher peak. Results with the lateral damage index Z_j^L are not conclusive. Results of damage scenario D5 presented in Figure 17 demonstrate the capability of the lateral index to correctly identify the two damaged columns. In this case the results of the vertical damage index are not conclusive. Overall, as also discussed previously, the vertical damage index is able to locate beam element damage even in the multiple damage case and the lateral index is able to locate column element damages. This method also demonstrated the capability of the damage indices to estimate the relative damage severity.

The performance of each proposed damage index is summarized in Table 7. Since one damage index cannot reliably identify damage in all scenarios, the combined method can provide a better chance to cross check and obtain the correct results. Moreover when there is no previous information on the damage location, as what happen in real life, MMF could assist MMSE to confirm whether the damage is in a beam or a column element. MMF, $MMSE^L$ and $MMSE^V$ could then be used together to confirm damage location, as they will complement and supplement each other and the damage location can be determined with some confidence when at least two indicators confirm this.

Table 7 Performance of each damage indicator

Damage Scenario	MMF	MMSE	
	$\overline{\delta}\%_{(2L+V)}$	Z_j^L	Z_j^V
D1	√√	√√	×
D2	√√	×	√√
D3	√*	√√	√√
D4	√√	×	√√
D5	√*	√√	×

Note: √√ means accurate damage localization; √* means partly damage indication; × means false indication.

5. CONCLUSIONS

A procedure to detect and locate damage in an asymmetric building structure has been developed and presented in this paper. It uses a multi-criteria approach (MCA) to complement and supplement the results of MMF and MMSE methods to obtain reliable outcomes. The contribution of this research can be captured by the process that was developed in three stages; firstly, the traditional MF method is modified to fit the three dimensional asymmetric building structures. Then, Stubbs' MSE index is modified by decomposing it into two indices (1) vertical damage index and (2) lateral damage index so that damage in the horizontal elements of an asymmetric building structure can also be detected in addition to that in the vertical elements. The last stage is to incorporate all the proposed damage indices in the damage detection procedure so that the results can be compared to provide the best chance of obtaining reliable results in damage detection.

This procedure was first illustrated through its application to a 2 story setback asymmetric building model, which also enabled the validation of the modelling techniques. This was followed by numerical simulations, under a range of damage scenarios, in a 10 story L-shape asymmetric building structure. A total of five damage scenarios were considered in the numerical simulations, two single damage scenarios with damage in beam and column and three multiple damage scenarios with damage in both a column and a beam, multi-beam damages or multi-column damages. The results showed that the MMF method can accurately locate beam damage, but when the damaged member is a column in a multiple damage case, this damage is unlikely to be identified clearly. MMSE method, using the vertical or the horizontal damage index is capable of locating the damage in either a horizontal beam or a vertical column respectively. However, as there will be no prior knowledge of the damage location in real life, the MMF method can be a good indicator to confirm whether the damage is in a beam or a column element. As there are some discrepancies in each method, the MCA incorporating the three proposed damage indices will be useful for accurate damage detection. The procedure developed in this research can be extended to detect and locate damage in different types of asymmetric buildings, normal high-rise buildings, multi-propose towers, etc.

ACKNOWLEDGMENTS

This paper forms a part of a continuing study of structural health monitoring of structures conducted at the Queensland University of Technology, Australia. Yi Wang gratefully acknowledges the support of this research provided by the Queensland University of Technology Postgraduate Research Award and International Postgraduate Research Scholarship.

REFERENCES

1. Chan, T.H., et al., *Structural health monitoring for long span bridges: Hong Kong experience and continuing onto Australia*, in *Structural Health Monitoring in Australia*, T.H. Chan and D.P. Thambiratnam, Editors. Nova Science Publishers, Inc.: New York. **2011**, p. 1-32.
2. Dowling, L. and G. Rummey, Guidelines for Bridge Management: Structure Information. **2004**.
3. Kaphle, M., et al., Identification of acoustic emission wave modes for accurate source location in plate-like structures. *Structural control and health monitoring*, **2012**. 19(2): p. 187-198.
4. Balageas, D., C.-P. Fritzen, and A. Güemes, *Structural health monitoring*. Vol. 493. Wiley Online Library. **2006**.
5. Rizos, P., N. Aspragathos, and A. Dimarogonas, Identification of crack location and magnitude in a cantilever beam from the vibration modes. *Journal of sound and vibration*, **1990**. 138(3): p. 381-388.
6. Hong, J.-C., et al., Damage detection using the Lipschitz exponent estimated by the wavelet transform: applications to vibration modes of a beam. *International journal of solids and structures*, **2002**. 39(7): p. 1803-1816.
7. Shih, H.W., D.P. Thambiratnam, and T.H. Chan, Vibration based structural damage detection in flexural members using multi-criteria approach. *Journal of sound and vibration*, **2009**. 323(3): p. 645-661.
8. Cornwell, P., S.W. Doebling, and C.R. Farrar, Application of the strain energy damage detection method to plate-like structures. *Journal of Sound and Vibration*, **1999**. 224(2): p. 359-374.
9. Messina, A., T. Contursi, and E.J. Williams, A Multiple-Damage Location Assurance Criterion Based on Natural Frequency Changes. *Journal of Vibration and Control*, **1998**. 4: p. 619-633.
10. Shi, Z., S. Law, and L. Zhang, Damage localization by directly using incomplete mode shapes. *Journal of Engineering Mechanics*, **2000**. 126(6): p. 656-660.
11. Law, S., Z. Shi, and L. Zhang, Structural damage detection from incomplete and noisy modal test data. *Journal of Engineering Mechanics*, **1998**. 124(11): p. 1280-1288.
12. Wang, S., et al. Comparative study of modal strain energy based damage localization methods for three-dimensional structure. in *The Twentieth International Offshore and Polar Engineering Conference*. **2010**. International Society of Offshore and Polar Engineers.
13. Liu, F., et al., Experimental study of improved modal strain energy method for damage localisation in jacket-type offshore wind turbines. *Renewable Energy*, **2014**. 72: p. 174-181.
14. Li, H., H. Yang, and S.-L.J. Hu, Modal strain energy decomposition method for damage localization in 3D frame structures. *Journal of engineering mechanics*, **2006**. 132(9): p. 941-951.

15. Hu, J.S.-L., S. Wang, and H. Li, Cross-modal strain energy method for estimating damage severity. *Journal of engineering mechanics*, **2006**. 132(4): p. 429-437.
16. Xiaodong, J., Q. Jiaru, and X. Longhe, Damage diagnosis of a two-storey spatial steel braced-frame model. *Structural Control and Health Monitoring*, **2007**. 14(8): p. 1083-1100.
17. Morita, K., M. Teshigawara, and T. Hamamoto, Detection and estimation of damage to steel frames through shaking table tests. *Structural Control and Health Monitoring*, **2005**. 12(3-4): p. 357-380.
18. Shih, H.W., D. Thambiratnam, and T.H. Chan, Damage detection in truss bridges using vibration based multi-criteria approach. *Structural Engineering and Mechanics*, **2011**. 39(2): p. 187.
19. Wang, F.L., et al., Correlation-based damage detection for complicated truss bridges using multi-layer genetic algorithm. *Advances in Structural Engineering*, **2012**. 15(5): p. 693-706.
20. Shih, H., D. Thambiratnam, and T. Chan, Damage detection in slab-on-girder bridges using vibration characteristics. *Structural Control and Health Monitoring*, **2013**. 20(10): p. 1271-1290.
21. Ueng, J.-M., C.-C. Lin, and P.-L. Lin, System identification of torsionally coupled buildings. *Computers & Structures*, **2000**. 74(6): p. 667-686.
22. Fan, W. and P. Qiao, Vibration-based damage identification methods: a review and comparative study. *Structural Health Monitoring*, **2011**. 10(1): p. 83-111.
23. Farrar, C.R. and H.Y. Sohn, Condition/damage monitoring methodologies. **2001**, Los Alamos National Laboratory.
24. West, W.M. Illustration of the use of modal assurance criterion to detect structural changes in an orbiter test specimen. in *International Modal Analysis Conference, 4 th, Los Angeles, CA, Proceedings.* **1986**.
25. Ko, J., C. Wong, and H. Lam. Damage detection in steel framed structures by vibration measurement approach. in *Proceedings of the 12th International Modal Analysis*. **1994**.
26. Cempel, C., H. Natke, and A. Ziolkowski, Application of transformed normal modes for damage location in structures, in *Structural integrity assessment*. **1992**. p. 246-255.
27. Pandey, A. and M. Biswas, Damage detection in structures using changes in flexibility. *Journal of sound and vibration*, **1994**. 169(1): p. 3-17.
28. Wang, B.S., et al., Comparative study of damage indices in application to a long-span suspension bridge, in *Advances in Structural Dynamics*, J.M.K.a.Y.L. Xu, Editor. **2000**, Elsevier Science Ltd: Oxford, UK. p. 997-1004.
29. Sung, S., K. Koo, and H. Jung, Modal flexibility-based damage detection of cantilever beam-type structures using baseline modification. *Journal of Sound and Vibration*, **2014**. 333(18): p. 4123-4138.
30. Stubbs, N., J.-T. Kim, and C. Farrar. Field verification of a nondestructive damage localization and severity estimation algorithm. in *Proceedings-SPIE the international society for optical engineering*. **1995**. SPIE INTERNATIONAL SOCIETY FOR OPTICAL.
31. Stubbs, N. and J.-T. Kim, Damage localization in structures without baseline modal parameters. *Aiaa Journal*, **1996**. 34(8): p. 1644-1649.
32. Shi, Z., S. Law, and L. Zhang, Structural damage localization from modal strain energy change. *Journal of Sound and Vibration*, **1998**. 218(5): p. 825-844.
33. Berman, A. and W.G. Flannelly, Theory of incomplete models of dynamic structures. *AIAA journal*, **1971**. 9(8): p. 1481-1487.

34. Wickramasinghe, W.R., et al., Vibration characteristics and damage detection in a suspension bridge. *Journal of Sound and Vibration*, **2016**. 375: p. 254-274.
35. ANSYS Inc., ANSYS Mechanical APDL Academic Research. **2011**: Canonsburg PA.
36. Li, H., H. Fang, and S.-L.J. Hu, Damage localization and severity estimate for three-dimensional frame structures. *Journal of Sound and Vibration*, **2007**. 301(3): p. 481-494.